https://doi.org/10.1016/j.apcata.2017.10.012

The effect of synthesis parameters on ordered mesoporous nickel alumina catalyst for CO_2 methanation

Ali Aljishi, Gabriel Veilleux, Jose Augusto Hernandez Lalinde, Jan Kopyscinski*

Department of Chemical Engineering, McGill University,

3610 University Street, Montreal, Quebec H3A 0C5, Canada

* To whom all correspondence should be addressed:

Tel.: +1 514 398 4276

jan.kopyscinski@mcgill.ca

Graphical abstract

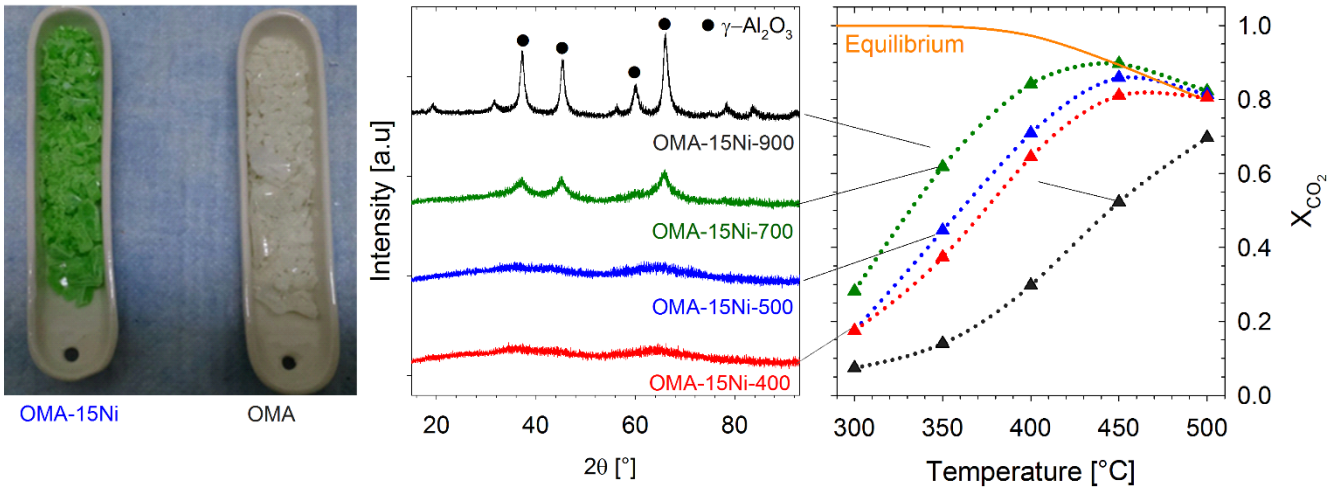

Abstract

A series of ordered mesoporous nickel alumina catalysts were synthesized via the evaporation induced self-assembly technique (EISA). Varying synthesis parameters such as the type of acid, nickel loading, calcination temperature as well as synthesis method influenced the catalyst morphology and its activity towards CO_2 methanation. Catalyst prepared without acid formed macroporous structures with a very low surface area (47 m^2 g^{-1}), whereas using a mixture of hydrochloric and citric acid resulted in incomplete formation of mesoporous micelles with surface area of 173 m^2 g^{-1}. On the other hand, using nitric acid lead to complete formation of long cylindrical micelles with a combined surface areas up to 260 m^2 g^{-1} and highly dispersed nickel clusters with a size of 3-5 nm. An optimum calcination temperature of 700°C was determined yielding the highest CO_2 conversion and CH_4 selectivity. This catalyst displayed a stable performance and did not exhibit any sign of deactivation during a 150 h test. Catalysts calcined at lower and higher temperatures had smaller surface areas as well as lower catalytic activity.

Keywords: CO_2 methanation • Ordered mesoporous nickel alumina catalyst • Catalyst synthesis and characterization

1 Introduction

Energy storage is a burning topic in the development of renewable energies such as wind and solar, mainly due to the intermittencies of electricity production. Growing interest has been observed towards the Power-to-Gas process (P2G) in which excess electrical energy is used to produce hydrogen via water-electrolysis, which is subsequently converted with captured CO_2 to grid compatible gas (methane). The P2G process combines electricity storage and CO_2 utilization leading potentially to a closed carbon cycle (Circular Economy)[1]. Beside water-electrolysis, the methanation is the most important and technically challenging step in the P2G process. Current areas of research focus on (1) evaluating suitable carbon oxides sources (i.e., biogas, power plants, extraction from air), (2) catalyst design, and (3) reactor and process design including heat integration.

The main overall reactions are the CO_2 methanation (eq. 1), the competing reverse water-gas-shift reaction (eq. 2), which leads to undesired CO, and the subsequent CO methanation (eq.3).

$$CO_2 + 4H_2 \rightarrow CH_4 + 2H_2O \qquad \Delta H_R^o = -165\ kJ\ mol^{-1} \tag{1}$$

$$CO_2 + H_2 \leftrightarrow CO + H_2O \qquad \Delta H_R^o = 41\ kJ\ mol^{-1} \tag{2}$$

$$CO + 3H_2 \leftrightarrow CH_4 + H_2O \qquad \Delta H_R^o = -206\ kJ\ mol^{-1} \tag{3}$$

The reactions involved are catalyzed by supported Ni, Ru, and Rh systems of which the latter two noble metals are more active than Ni-based catalysts [2–4]. Nickel might still be the first-choice due to lower costs and its high catalyst stability shown for syngas/CO methanation (eq.3) [5]. For the CO_2 methanation, however, the stability of Ni-catalysts is not proven on a commercial scale.

New catalysts have been developed of which the ordered mesoporous alumina catalysts (OMA) show great promise due to larger surface areas, larger pore volumes and uniform pore size distribution compared to traditional catalyst systems allowing for a better interaction between the metal-oxide and the support resulting a high metal dispersion [6,7]. In addition, the metallic nanoparticles are stabilized

due to the confinement effect of the mesoporous framework that suppresses sintering and agglomeration of the metal atoms (e.g., Ni) even at high reaction temperatures. Therefore, ordered mesoporous alumina materials are considered an ideal catalyst support for reforming [7–9], oxidation [10,11] and hydrogenation [12] reactions.

Ordered mesoporous alumina catalysts can be synthesized by various methods as outlined in [13–15]. The “one-step” facile route with evaporation induced self-assembly (EISA) has become one of the most adopted techniques due to its simple and flexible procedure [14,15]. In EISA, the precursors are mixed together at the desired concentrations until a homogeneous solution is obtained, which is then dried and calcined. A polymeric surfactant/copolymer is often used as soft template and mixed with a polar organic solvent and acid. Using a non-polar solvent like toluene would result in a water-in-oil emulsion and would lead to rod formation rather than a mesoporous structure. Providing an acidic environment is key in inducing the mesoporous structure since the polymerization and cross-linking rate are too fast at a pH of 6-8.5 [14,15]. Nitric acid as well as mixtures of hydrochloric and citric acid have been used in the synthesis of alumina and silica based catalysts. Besides the acidic environment, the calcination temperature influences the catalyst structure and morphology hence its activity as observed for the partial oxidation of methane [11].

Recently, Ni-OMA catalysts were tested for CO_2 methanation and showed higher CO_2 conversion and CH_4 selectivity compared to non-mesoporous nickel alumina catalysts [12]. Considering the promising results, this work deals with the development of alumina based ordered mesoporous catalysts using EISA synthesis method with various synthesis parameters. The objective was to study the effect of different Ni loadings, calcination temperatures, and the acid used on the catalyst morphology and activity towards the CO_2 methanation at different reaction temperatures and gas hourly space velocities.

2 Experimental

2.1 Catalyst Preparation

EISA technique was chosen as it was reported to be a robust mesoporous catalyst synthesis pathway**.** Approximately 1 g of triblock copolymer (Pluronic® P-123, Sigma Aldrich) was dissolved in 20 ml of anhydrous ethanol until a homogeneous solution was obtained. Subsequently 2-4 g of aluminum-isopropoxide (≥ 98%, Sigma Aldrich) and up to 1.5 g of nickel (II) nitrate hexahydrate (≥ 98.5%, Sigma Aldrich) were added to achieve the desired catalyst mass and nickel target loadings (Table 1). Nitric acid (68 wt%, Fisher Scientific) or a mixture of hydrochloric (37 wt%, Fisher Scientific) and citric acid (Sigma Aldrich) was then added to provide the acidic environment to enhance mesopore formation. The solution was stirred for 5 h at 600 rpm at room temperature. The homogenized solution obtained, was dried at 60°C for 48 h and subsequently calcined in a muffle furnace with heating rate of 1°C min^{-1} for 5 h at the targeted calcination temperature (i.e., 400, 500, 700 or 900°C).

Samples with three different nickel loadings (5 wt%, 15 wt% and 30 wt%) and four different calcination temperatures (400-900°C) were prepared. The catalysts were named OMA-15Ni-500, where OMA refers to ordered mesoporous alumina, 15Ni refers to the nickel loading in wt% and 500 to the calcination temperature in degree Celsius (°C). OMA-500 denotes to the support only, calcined at 500°C; whereas catalysts prepared without no acid or with hydrochloric + citric acid, were labeled OMA-500-No Acid or OMA-500-HCl and OMA-15Ni-500-HCl, respectively (Table 1).

In addition, a 15 wt% Ni/OMA catalyst was synthesized via wet impregnation for comparison. First, the OMA support was prepared via the aforementioned technique and calcined at 500°C. Secondly, the OMA support was added slowly to the nickel (II) nitrate hexahydrate solution and stirred vigorously (~600 rpm) for 6 h. The mixture was dried for 24 h at 100°C and then calcined at 500°C with heating rate of 1°C min^{-1} for 5 h. The catalyst was named 15Ni/OMA-500.

All of the produced catalyst samples were sieved into three different particle size categories (45-90 µm, 90-125 µm, and 125-150 µm) using a DUAL D-4326 motorized sieve.

2.2 Catalyst Characterization

Various characterization techniques were used to study catalyst morphology, crystallinity and composition. Sieved particles with 45-90 µm were used in all characterization techniques, whereas particles of 125-150 µm were used in H_2 temperature programmed reduction and activity measurements. Inductively Coupled Plasma - Optical Emission Spectroscopy (ICP-OES, iCAP 6500 dual view Thermo Scientific) was used to assess the actual nickel concentration in each sample. Prior to the analysis, 100 mg of the catalyst sample was digested in a mixture of 2 ml of nitric acid (67 wt%, Fisher Scientific) and 3 ml of hydrochloric acid (37 wt%, Fisher Scientific) at 95°C for 3 h.

N_2 adsorption/desorption measurements (-196°C) were conducted using Micromeritics Tristar 3000 BET analyzer to determine total surface area, pore size distribution and pore volume. Before the analysis, the samples were degassed under vacuum for 12 h at 200°C.

X-Ray Diffraction (XRD) was used to identify the crystallinity of the catalyst. Analyses were conducted on a Bruker D8 Discovery X-Ray Diffractometer with two-dimensional VANTEC-500 detector and CuK_α (λ = 1.54056 Å) radiation source. The measurements were done with a scan rate of 5° min^{-1} at a tube voltage of 40 kV and a tube current of 20 mA.

Temperature program reduction (H_2-TPR) experiments were carried out in fixed bed reactor setup coupled with a calibrated mass spectrometer (Pfeiffer Omnistar GSD 301). Approximately, 100 mg of fresh calcined catalyst was heated under Ar atmosphere (40 ml_N min^{-1}, 99.999%, Megs) with a rate of 10°C min^{-1} to 310°C for 3 h to remove moisture. After cooling the sample to room temperature, H_2 (99.999%, Megs) was introduced and the sample was heated at a rate of 8.5°C min^{-1} to 950°C while the

corresponding mass to charge ratio for H_2O (m/z = 18) was recorded. Flow rates of H_2 and Ar were respectively set to 10 and 40 $ml_N\ min^{-1}$ (subscript *N* denotes normal condition with T = 0°C and 1 bar). Temperature programmed oxidation was carried out for both fresh and spent OMA-15Ni-700 (used at 400 °C for 150 h) catalysts using a thermogravimetric analyzer (TGA, Q500 TA instrument). Note, the fresh catalyst was calcinated, while the spent catalyst was passivated after the long-term experiment. Approximately, 9 mg of sample was placed in the TGA and heated in presence of N_2 to 130°C at the rate of 5°C min^{-1}, while the weight change was recorded. After a holding time of 30 minutes to remove moisture, the sample was then heated in Air to 900°C at 5°C min^{-1} to combust possible carbon deposition. Volumetric hydrogen uptake (chemisorption) was conducted in an Autosorb iQ (Quantachrome) gas sorption instrument. Approximately 100 mg of fresh calcined sample was placed in a U-shaped quartz tube, preheated in He at 120°C with a heating rate of 20°C min^{-1} for 0.5 h, then reduced with H_2 (5 vol% H_2 in He or 100 vol% H_2) at its optimum reduction temperature obtained from H_2-TPR for another 3 h, then evacuated for 1 h and subsequently cooled to 40°C, where all adsorption measurements were taken at pressures ranging from 0.05 bar to 0.8 bar. Specific surface area ($m^2\ g^{-1}$), metal dispersion (*D* in %) and average crystallite size (*d* in nm) were calculated based on the amount of H_2 adsorbed assuming an atomic stoichiometric ratio of H/Ni = 1 and a hemispherical cluster with a nickel density of 8.9 $g\ cm^{-3}$. Transmission electron microscopy (TEM) of fresh and calcined catalyst was carried out on FEI Tecnai G2 F20 with 200 kV. Prior to the analysis, a thin (100 nm) section of the catalyst was prepared using a dual-beam focused ion beam (FEI Helios 600 NanoLab, Hillsboro) equipped with a gallium ion source. The ICP-OES, H_2-TPR, N_2-physisorption and H_2-chemisorption analyses were repeated at least twice for each batch to assure that catalysts prepared with the same recipes at different days had the same properties.

2.3 Activity Measurements

The catalyst performance was tested in a fixed bed reactor (FBR) system at atmospheric pressure. The setup included mass flow controllers, gas mixing station, tube furnace, condenser and gas analyzer (mass spectrometer). The reactant gases, Ar (99.999%, Megs), H_2 (99.999%, Megs) and CO_2 (99.99%, Praxair), were mass flow controlled using calibrated Vögtlin red-y smart controller GSC (Switzerland). The reactor was stainless steel (SS316) with a double tube counter-current flow configuration. The inner tube (ID = 4.57 mm) was closed with a 5 μm thick stainless steel frit on which the catalyst was placed. The exit gas line was electrically heated between 150-180°C to avoid condensation of water. A split stream of the exit gas was analyzed using a calibrated mass spectrometer (Pfeiffer Omnistar GSD 301), while the rest of the exit gas was exhausted after condensation. The experiments were performed in the 300 to 500°C temperature range with gas hourly space velocities (GHSV) ranging from 45-115 $L_N\ g_{cat}^{-1}\ h^{-1}$. The reaction temperature was controlled by a K-type thermocouple inserted into the catalyst bed. Prior to the experiments, the catalysts were reduced with 20 vol% H_2 in Ar for 3 h at their respective reduction temperature determined via H_2-TPR. The reactions were performed at 1 bar with H_2/CO_2 ratio of 5:1. Argon gas was used as an internal standard. The catalyst was subjected to each experimental condition for at least 3 h. The OMA-15Ni-700 catalyst was used in a 150 h long-term run to study the catalyst stability. The test was performed at 400°C with a GHSV of 91 $L_N\ g_{cat}^{-1}\ h^{-1}$. After the reaction, all catalysts were passivated and then removed, stored and analyzed.

Conversion of carbon dioxide (X_{CO2}), and product selectivity (S_i) were defined per eqs. 4 and 5.

$$X_{CO_2} = \frac{\dot{n}_{CO_{2,in}} - \dot{n}_{CO_{2,out}}}{\dot{n}_{CO_{2,in}}} \quad (4)$$

$$S_i = \frac{\dot{n}_i}{\dot{n}_{CO_{2,in}} - \dot{n}_{CO_{2,out}}} \quad (5)$$

Where $\dot{n}_i$ is the molar flow rate of species *i* (i.e., CH_4, CO). Only CH_4 and CO, but no C_2+ hydrocarbons were detected during all activity experiments.

To ensure the reproducibility of the results, three different batches of the catalysts (e.g., OMA-15Ni-500) were synthesized using the exact procedures and tested in the reactor under the same conditions and reduced at the same temperature. The results (CO_2 conversion and CH_4 selectivity) varied within ± 3 % and were very small compared to the change in conversion and selectivity obtained for different catalysts.

3 Results and Discussion

3.1 Characterization of fresh catalyst

3.1.1 N_2 Adsorption/desorption analysis

N_2 adsorption/desorption isotherms and the pore size distributions of the synthesized supports and nickel catalysts are depicted in Fig. 1. All the samples prepared with nitric acid showed a type-IV isotherm with H1 hysteresis loop, indicating the formation of uniform cylindrical mesoporous structure [11]. Acidic media were important in creating mesoporous structure; samples prepared without acid did not exhibit a type-IV isotherm (Figure 1A and B labeled OMA-500-No Acid) and had a very small total surface of 47 $m^2\,g^{-1}$, of which 43 $m^2\,g^{-1}$ was macroporous (Table 1). Lack of acidity in the synthesis media resulted in low tendency towards mesopore formation as the copolymer became less hydrophilic [16].

The type of acid used during the synthesis played an important role in the formation of organized mesoporous structures. The catalyst prepared with hydrochloric and citric acid had a smaller mesoporous surface area (134 m^2g^{-1} for OMA-500-HCl) compared to the one prepared with nitric acid (258 $m^2\,g^{-1}$ for OMA-500), see Table 1. This might be related to the role of anion (e.g., NO^{3-}, Cl^-) and their binding strengths when adsorbed on the positively charged surfactant during the synthesis [17]. The binding strength of NO^{3-} ions was sufficient to promote long micelles, hence, a more ordered and organized structure.

Table 1 Sample overview: Synthesis parameter (target Ni loading, calcination temperature T_{cal}, acid used) and N_2 adsorption/desorption results (total and mesoporous surface area, average pore size, pore volume).

Sample	***Ni* [wt%]**	T_{cal} **[°C]**	***Acid used***	S_{BET} [a] **[$m^2 g^{-1}$]**	S_{Meso} [b] **[$m^2 g^{-1}$]**	D_{Pore} [c] **[nm]**	V_{Pore} [d] **[$cm^3 g^{-1}$]**
OMA-500-No Acid	0	500	none	47	43*	11.6	0.14
OMA-500-HCl	0	500	HCl+CA	173	134	7.2	0.31
OMA-400	0	400	HNO_3	175	153	14.0	0.60
OMA-500	0	500	HNO_3	262	258	8.0	0.52
OMA-700	0	700	HNO_3	202	190	8.3	0.42
OMA-15Ni-400	15	400	HNO_3	140	124	11.7	0.41
OMA-15Ni-500	15	500	HNO_3	242	234	10.0	0.60
OMA-15Ni-700	15	700	HNO_3	206	198	8.2	0.42
OMA-15Ni-900	15	900	HNO_3	123	115	8.9	0.28
OMA-05Ni-500	5	500	HNO_3	217	206	9.4	0.52
OMA-30Ni-500	30	500	HNO_3	174	168	12.7	0.58
15Ni/OMA-500	15	500	HNO_3	135	122	8.5	0.29
OMA-15Ni-500-HCl	15	500	HCl+CA	83	72	12.7	0.25

[a] S_{BET} = BET total specific surface area obtained from adsorption data in the p/p^0 range from 0.05-0.2; all reported data are within ± 4 $m^2 g^{-1}$ based on repeated analysis. [b] S_{Meso} = mesoporous surface area determined via subtracting the microporous surface area. [c] D_{Pore} = average pore diameters calculated using Barrett-Joyner-Halenda (BJH) method; [d] V_{Pore} = pore volume was obtained at p/p^0 = 0.97; * macropores.

Surface area and pore volume were influenced by the calcination temperature and catalyst loading as depicted in Figure 1C to H. The maximum mesoporous surface area for support (258 $m^2 g^{-1}$ for OMA-500) and nickel catalyst (234 $m^2 g^{-1}$ for OMA-15Ni-500) was found for a calcination temperature of 500°C (Table 1). Calcination temperatures of 400 or 900°C yielded a much smaller surface area of 153 to 115 $m^2 g^{-1}$ for samples with and without nickel (Table 1). Interestingly, the surface area for the samples calcined at 400°C exhibited a bimodal pore size distribution (Figure 1D and F), probably due to the incomplete combustion of the soft template (P123 copolymer). The reduction in surface area and pore volume for the samples calcined at 900°C might be associated with the reconstruction of the surface and/or thermal collapsing of the mesoporous structure.

A temperature of 500°C for the calcination has been used as basis to investigate the influence of the nickel loading. Adding nickel reduced the mesoporous surface area slightly (e.g., 258 $m^2 g^{-1}$ and 234 $m^2 g^{-1}$ for OMA-500 and OMA-15Ni-500, respectively). However, calcined at 700°C the sample with and without nickel had about the same mesoporous surface area of 194 ± 4 $m^2 g^{-1}$. In contrast, adding nickel to the solution containing hydrochloric and citric acid during the synthesis reduced the total surface area significantly from 173 to 83 $m^2 g^{-1}$ (OMA-500-HCl and OMA-15Ni-500-HCl), implying that nitric acid is a better reagent. Similar results have been reported for mesoporous silica materials [17]. Using hydrochloric and citric acid might require a much longer induction time.

Increase in nickel loading to 30 wt% led to a decrease in the mesoporous surface area, larger pores and less uniform pore size distribution (Table1 and Figure 1H).

The catalyst prepared via impregnation (15Ni/OMA-500) had a mesoporous surface area of 122 $m^2 g^{-1}$, which is significantly smaller than 234 $m^2 g^{-1}$ for OMA-15Ni-500. A considerable number of pores might be blocked by adding nickel clusters to mesoporous framework. Thus, following the EISA technique yielded in highly organized samples with larger surface areas compared to the sample prepared via impregnation.

3.1.2 ICP analysis

ICP-OES was used to confirm the presence of nickel in the catalysts. Results showed that the actual nickel loadings were close to the targeted theoretical values indicating an effective synthesis of the ordered mesoporous nickel alumina catalyst (Table 2).

Table 1 Target and actual nickel loadings for ordered mesoporous catalysts determined by ICP-OES.

Catalyst Code	Target [wt%]	Actual [wt%]
OMA-05Ni-500	5.0	4.7 ± 0.1
OMA-15Ni-500	15.0	13.5 ± 1.3
OMA-30Ni-500	30.0	28.6 ± 3.2

3.1.3 TEM analysis

The fresh and calcined OMA-15Ni-500 catalyst was analyzed with TEM. During the preparation, the catalyst was cut with a focused ion beam along the axis of the pores and not perpendicular. Thus, the typical hexagonally shape of the pores with p6mm symmetry could not be confirmed. However, aligned cylindrical pores were clearly visible (Fig. 2 A and B). The average pore diameter determined with nitrogen physisorption measurements was 9-11 nm and smaller than observed via TEM. Here, the cylindrical micelles had a diameter between 50-100 nm containing multiple holes in the wall along the axis with approximately 10-20 nm in diameter. Highly dispersed nickel clusters with a crystallite sizes between 2 to 5 nm were observed as well (Fig. 2C), which were much smaller compared to values reported in the literature [18], but similar to the values determined via hydrogen chemisorption (see section 3.1.5). Analysis with an image processing software (ImageJ) showed that the average nickel crystallite size was around 2.8 nm.

3.1.4 H_2-TPR analysis

Temperature programmed reduction (H_2-TPR) was used to investigate the interactions between nickel and the alumina support. The H_2O signal (m/z = 18) was monitored and recorded by mass spectrometry. The OMA-Ni catalysts calcined at 500°C exhibited a single reduction peak between 575°C and 620°C depending on the nickel loading (Fig. 3A). The influence of calcination temperature was studied for the OMA-15Ni catalyst. A broader H_2O peak at around 550°C was observed for the OMA-15Ni-400 compared to the OMA-15Ni-500 (Fig. 3B). At calcination temperatures of 700°C and 900°C, the TPR peaks shifted to higher temperatures of 780°C and 870°C, respectively, indicating a stronger interaction of the nickel with the alumina support. Small peaks appeared between 400-500°C for both catalysts calcined above 700°C. This small reduction peak might correspond to weak NiO interaction with the OMA support. TPR measurements were also conducted on the support (OMA-500), but did not result in

248 any H_2O formation (not shown), which verifies that the observed peaks are related to the reduction of
249 NiO only.

250 *3.1.5 H_2-uptake*

251 The mesoporous surface area of the OMA support impregnated with nickel (15Ni/OMA-500) was about
252 half of that for the sample prepared with the one-pot EISA method (OMA-15Ni-500, Table 1), but had a
253 25% higher H_2-uptake and specific surface area (Table 3, 179 vs. 142 µmol g^{-1}, 14 vs. 11 m^2 g^{-1}) for the
254 same nickel loading. This might suggest that some nickel atoms were encapsulated by the alumina
255 framework during the one-pot synthesis and not accessible. The sample synthesized with hydrochloric
256 and citric acid had a much smaller H_2-uptake and specific surface area (Table 3, 30 µmol g^{-1} and 2.3 m^2
257 g^{-1}), demonstrating that the type of acid used is important for both the formation of the mesoporous
258 structure and distribution of the active metal.

259 Table 3 H_2-uptake [µmol g^{-1}], specific surface area [m^2 g^{-1}], average nickel crystallite size [nm] and
260 metal dispersion [%].

Catalyst Code	**H_2-uptake [µmol g^{-1}][a]**	**Specific surface area [m^2 g^{-1}][a]**	**Crystallite size, *d* [nm][b]**	**Metal dispersion, *D* [%][b]**
OMA-15Ni-500	142	11.1	4.1	11.1
15Ni/OMA-500	179	14.0	3.2	14.3
OMA-15Ni-500-HCl	30	2.3	19.4	2.6
OMA-15Ni-400	166	13.0	3.5	13.3
OMA-15Ni-700	144	11.3	4.0	11.5
OMA-15Ni-900	96	7.5	6.1	7.7
OMA-05Ni-500	32	2.6	6.2	8.2
OMA-30Ni-500	295	23.1	4.2	12.1
OMA-15Ni-500*	152	11.9	3.8	12.2

[a] based on replicated analyses all values for H_2-uptake and specific surface area are within ± 8 µmol g^{-1} and ± 0.6 m^2 g^{-1}, respectively. [b] based on ICP measurements (total nickel content) the values reported for the average nickel crystallite size and metal dispersion are within *d* ± 0.4 nm and *D* ± 1.1 % (absolute), respectively. * reduced with 100% H_2;

261

The effect of the calcination temperature on the H_2-uptake shows that with higher temperature the H_2-uptake decreased from 166 to 96 µmol g^{-1}, while the average crystallite size increased from 3.5 to 6.1 nm for OMA-15Ni-400 to OMA-15Ni-900 (Table 3). The crystallite size determined with TEM were in the same range and matched nicely with the H_2-chemisoption measurements.

The H_2-uptake increased as expected with the nickel loading from 32 to 295 µmol g^{-1} for OMA-05Ni-500 to OMA-30Ni-500. However, the average crystallite size decreased slightly from 6.2 to 4.2 nm. In most cases, an increase in the metal loading results in an increase of the crystallite size, but for the ordered mesoporous catalyst prepared via EISA technique the opposite was observed. Again, this suggest that some nickel atoms were encapsulated by the alumina framework during the one-pot synthesis, especially for the OMA-05Ni-500 sample with a high alumina/nickel ratio. A minimum amount of nickel might be needed to achieve a good distribution and dispersion.

Prior to the chemisorption, the samples were reduced with 5 vol% H_2 in He at its TPR-peak temperature (see section 3.1.4) for 3 h. For comparison, the OMA-15Ni-500* sample was reduced with 100 vol% H_2 prior to the chemisorption measurement to assure a complete removal of the oxygen and formation of the active zero-valent nickel ($NiO + H_2 \rightarrow Ni + H_2O$). Both catalysts reduced with 5 vol% and 100 vol% H_2 had a comparable H_2-uptake and average crystallite size (i.e., 142 vs. 152 µmol g^{-1} and 4.1 vs. 3.8 nm), indicating a similar degree of catalyst reduction.

3.1.6 XRD analysis

Fig. 4 shows the XRD patterns of the catalysts synthesized using different methods, calcination temperatures and nickel loadings. Reference patterns for $NiAl_2O_4$, NiO and γ-Al_2O_3 are also shown for comparison and taken from the International Centre for Diffraction Data (ICDD) with the powder diffraction file (PDF) #010-0339, #044-1159 and #050-074, respectively. Samples prepared via wet impregnation (15Ni/OMA-500) and with hydrochloric acid (OMA-15Ni-500-HCl) exhibited distinct and sharp NiO diffraction peaks (Fig. 4A), representing a higher degree of crystallinity compared to the

OMA-15Ni-500 sample. For the latter, the absence of specific $NiAl_2O_4$, NiO and γ-Al_2O_3 peaks indicate that alumina and nickel were homogenously mixed and amorphous in nature. The same was observed for the sample calcined at 400°C (Fig. 4B). When the calcination temperature was increased to 700°C, crystallinity of the support started to increase and small diffraction peaks were observed on the (3 1 1), (4 0 0) and (4 4 0) lattice planes of γ-alumina. The sample calcined at 900°C had a highly crystalline γ-alumina structure. However, the sample was not thermally stable as the surface area and pore volume dropped by 50% compared to sample calcined at 500°C (Table 1).

Diffraction peaks associated with NiO (i.e., 2θ = 37.2°, 43.2° and 62.8°; Fig. 4B) were very broad for the nickel containing catalysts, indicating amorphous structure. The diffraction peaks became more pronounced with higher nickel loadings and crystalline structure. Again, no peaks associated with $NiAl_2O_4$ were detected, even for the OMA-30Ni-500 sample.

To study the structural change during the synthesis, OMA-30Ni-500 was analyzed by XRD before and after calcination as well as in its reduced form. Prior to the calcination the dried catalyst showed only a small diffraction peaks for NiO (i.e., 2θ = 43.2°) and a broader peak at around 20-26° corresponding to carbon of the soft template (Fig. 5). The transition to wider and broader peaks at 2θ = 43.2° upon analysis of the calcined catalyst revealed the formation NiO, which was mostly reduced to Ni after 3 h under reduction conditions (T = 580°C). Only a small peak for NiO was observed at 37.2° as the catalyst was passivated. The peak at 2θ = 66° is associated with the crystal structure of Al_2O_3 that started to appear at temperatures higher than 500°C.

3.2 Activity measurements

3.2.1 Effect of synthesis parameter

As discussed in section 3.1, the synthesis method significantly influenced the catalyst properties and thus the catalytic activity. The catalyst prepared with nitric acid (OMA-15Ni-500) exhibited a higher catalytic activity towards CO_2 methanation over the temperature range of 300-500°C compared to the catalysts prepared via impregnation and with hydrochloric + citric acid, 15Ni/OMA-500 and OMA-15Ni-500-HCl, respectively (Fig. 6). Larger mesoporous surface area (234 vs. 122 vs 72 $m^2\ g^{-1}$) and larger pore volume (0.6 vs. 0.29 vs. 0.25 $cm^3\ g^{-1}$) of the OMA-15Ni-500 sample made the highly dispersed active nickel clusters easily accessible, which resulted in higher CO_2 conversions and CH_4 selectivities at every reaction temperatures (300-500°C) tested (Fig. 6A and B; Table 1). Even though the H_2-uptake of the impregnated catalyst (15Ni/OMA-500) was 25% higher than for the OMA-15Ni-500 sample (Table 3), the mesoporous surface area was 50% smaller leading to a lower CO_2 conversion. This indicates that both active and mesoporous surface area are important catalyst parameters.

The CO_2 conversion for the OMA-15Ni-500 increased until it reached a maximum close to the theoretical equilibrium conversion at a temperature of 450°C. Thereafter, the CO_2 conversion as well as the CH_4 selectivity declined following the equilibrium. At 450°C the OMA-15Ni-500 achieved its maximum CH_4 selectivity of 0.982 ± 0.01, whereas only a value 0.778 and 0.959 was attained at 300°C and 500°C, respectively. In all the experiments, no C_2+ and higher hydrocarbons were detected as illustrated with the MS signal at mass-charge ratio m/z = 0 to 45 in Fig. 7. Thermodynamically, temperatures lower than 400°C are favorable for a high CO_2 conversion, but due to kinetic limitations temperatures of 400 to 450°C were needed. In contrast, CO formation is favoured at higher temperatures; however, in the current study CO was produced at lower temperatures only. For example, at 300°C selectivity values of S_{CO} = 0.21, S_{CO} = 0.35 and S_{CO} = 0.56 were determined for OMA-15Ni-500, 15Ni/OMA-500 and OMA-15Ni-

500-HCl, respectively. Again, this shows clearly that the EISA synthesis with the use of nitric acid is the best method for this application.

The reaction mechanisms for the CO_2 and CO methanation differ slightly and depend not only on the catalyst (e.g., active metal, promoter, support) but also the operating conditions. No unified mechanism exists, rather, multiple reaction pathways have been proposed assuming different elementary steps and adsorbed surface intermediates [19]. For example, it has been hypothesized that the C-O bond cleavage occurs on the catalyst surface via direct dissociation (i.e., from $CO_{2,ads} \rightarrow CO_{ads} + O \rightarrow C_{ads} + O$) or via hydrogen-assisted dissociation (e.g., COH_{ads}, $HCOO_{ads}$ surface intermediate) [20–22]. For the latter, it is assumed that hydrogen lowers the energy of the C-O bond activation leading eventually to a C_{ads} or $CH_{x,ads}$ carbon surface intermediate, which is then stepwise hydrogenated to methane. The results of the current study might indicate, that at lower temperatures the CO_2 methanation proceeds via direct dissociation to form a CO_{ads} intermediate. CO_{ads} formation and desorption to CO seems to be faster than the stepwise hydrogenation to CH_4. However, without detailed analysis of the surface intermediates using for example diffuse reflectance FTIR (DRTIFS) experiments, no concrete conclusions about the reaction mechanism can be drawn.

3.2.2 Effect of calcination temperature

Catalytic activity also depends on the calcination temperature. With increasing calcination temperature from 400 to 700°C, the conversion of CO_2 as well as the selectivity of CH_4 for all reaction temperatures increased (Fig. 8). A further increase of the calcination temperature to 900°C, however, showed a huge decline of the catalytic activity. For example, at a reaction temperature of 350°C, the conversion of CO_2 increased from 0.374 to 0.618 for calcination temperatures of 400 to 700°C and then decreased to 0.140 for a calcination temperature of 900°C. The results are in good agreement with the surface area analysis in which the samples calcined at 400 and 900°C (OMA-15Ni-400 and OMA-15Ni-900) had the smallest mesoporous surface areas and pore volumes. Furthermore, the mesoporous structure of the OMA-15Ni-

353 900 catalyst became more crystalline as illustrated in Fig. 4B and the specific surface area was 30%
354 smaller than for the OMA-15Ni-500 and OMA-15Ni-700 sample (Table 3).

355 *3.2.3 Effect of nickel loading*

356 As the nickel loading increased from 5 wt% to 30 wt% the CO_2 conversion as well as the CH_4 selectivity
357 increased. For example, at 350°C CO_2 conversion values of 0.23, 0.45 and 0.69, and CH_4 selectivity
358 values of 0.783, 0.911 and 0.966 were determined for OMA-05Ni-500, OMA-15Ni-500 and OMA-30Ni-
359 500, respectively (Fig. 9). It is very likely, that the 30 wt% nickel catalyst provided more active sites
360 (confirmed with H_2-chemisorption measurements) for the competitive adsorption of hydrogen and thus
361 stepwise hydrogenation of the assumed CO_{ads} surface intermediate compared to the catalyst with a lower
362 nickel loadings. The current results do not allow the determination of the relative surface coverage of
363 each catalyst. For that steady-state isotopic transient kinetic analysis combined with diffuse reflectance
364 FTIR and mass spectrometry (SSITKA-DRIFTS-MS) experiments need to be conducted.

365 *3.2.4 Effect of chemical space velocity*

366 The influence of the gas hourly space velocity (GHSV) was investigated for the OMA-15Ni-700 catalyst
367 since it exhibited the best overall performance towards CO_2 methanation. The experiments were
368 performed at GHSV values from 45 to 115 $L_N\ g_{cat}^{-1}\ h^{-1}$. At temperatures, lower than 400°C the CO_2
369 conversion as well as the CH_4 selectivity declined with increasing GHSV. Whereas at 450 and 500°C the
370 opposite trend was observed. The highest CO_2 conversion and CH_4 selectivity was achieved for GHSV
371 of 45 $L_N\ g_{cat}^{-1}\ h^{-1}$ at 400°C. The GHSV values used in this study were considerably higher than those in
372 other reports such as 15 $L_N\ g_{cat}^{-1}\ h^{-1}$ in [12,23], but achieving similar high CH_4 selectivity values.

373 *3.2.5 Long-term experiment*

374 The OMA-15Ni-700 catalyst was subjected to a long-term run at 400°C with $H_2/CO_2 = 5$ at a GHSV of
375 91 $L_N\ g_{cat}^{-1}\ h^{-1}$. After continues operation of more than 150 h on stream, the catalyst did not exhibit any

sign of deactivation, the CO_2 conversion and CH_4 selectivity were stable with ~83% and 97%, respectively (Fig. 12 A).

3.3 Characterization of used catalyst

3.3.1 N_2 Adsorption/desorption analysis

BET surface area analysis was carried out for the spent catalysts with different nickel loadings. Surface area and pore volume of the spent catalysts were reduced by 40-50 $m^2\ g^{-1}$ and 0.02-0.06 $cm^3\ g^{-1}$ (Table 4), respectively. This might be associated with thermal shrinkage of the mesoporous framework and/or sintering of weakly interacted nickel clusters due to the high reduction temperatures of 575 to 620°C, which were considerably higher than the calcination temperature of 500°C and the reaction temperatures. However, this shrinkage did not lead to a collapse of the mesoporous structure as they showed type IV isotherms with H1-hysteresis and narrow pore size distributions (not shown), demonstrating good thermal stability of the mesoporous catalyst. The catalyst used for the 150 h test (OMA-15Ni-700), exhibited a similar reduction of surface area (by 30 $m^2\ g^{-1}$), confirming the excellent stability.

Table 4 BET surface area analysis for fresh and spent catalysts.

Sample	S_{BET} **($m^2\ g^{-1}$)**		V_{pore} **($cm^3\ g^{-1}$)**	
	fresh	*spent*	*fresh*	*spent*
OMA-05Ni-500	217	177	0.52	0.50
OMA-15Ni-500	242	191	0.60	0.54
OMA-30Ni-500	174	136	0.58	0.52
OMA-15Ni-700*	206	176	0.42	0.38

* used in 150 h long term experiment

3.3.2 XRD of used catalysts

XRD patterns of the spent catalysts of various nickel loadings are displayed in Fig.11. All the catalysts were subjected to reduction and reaction conditions as each catalyst was used for at least 3 consecutive days. The transformation of NiO to Ni can be observed clearly via XRD where the diffraction peaks of

Ni became obvious at higher Ni loadings (15-30 wt%) at 2θ = 44.4°, 51.8° and 76.3°. The diffraction peak at 66° for OMA-30Ni-500 corresponds to γ-Alumina which was most likely formed during the reduction.

3.3.3 Temperature programmed oxidation

To further investigate the catalyst stability, temperature programmed oxidation (TPO) of the fresh and used catalyst (150 h) were conducted. The fresh catalyst exhibited a weight reduction by 4 wt% on dry basis upon heating in Air to 500°C, which can be associated with the devolatilization of adsorbed species. A further increase in the temperature resulted in small weight increase for yet unknown reasons. The spent catalyst showed a completely different behavior; no weight decrease was measured. Instead, the weight of the used catalyst increased by approximately 3 wt% on dry basis in the range of 150 to 300°C with a total increase of 8.4 wt% at 900°C. This, result clearly demonstrates the absence of any carbon deposition and the oxidation of the passivated catalyst (i.e., 2 Ni + O_2 → 2 NiO).

4 Conclusions

A systematic approach was followed to investigate the relationship between the synthesis of nickel containing ordered mesoporous alumina catalysts and its structure and catalytic activity toward CO_2 methanation. Type of acid used, calcination temperature, nickel loading and synthesis method affected the catalyst morphology and activity significantly. Obtaining a complete mesoporous structure was the key for a good catalytic performance. Using nitric acid during the "one-step evaporation induced self-assembly - EISA" synthesis allowed the formation of long and cylindrical micelles with small and highly dispersed nickel clusters. Catalysts prepared via wet impregnation had smaller surface area and lower CO_2 methanation activity. Besides the acid used, the calcination temperature was one of the most important synthesis parameters. 700°C was found to be the optimum calcination temperature in the present study leading to large mesoporous and specific surface areas, and achieving the highest CO_2

conversion and CH_4 selectivity over the whole temperature range studied. In addition, the catalyst proved to be stable under reaction conditions for more than 150 h without any sign of deactivation.

Understanding how the synthesis parameters of ordered mesoporous alumina catalysts affect the CO_2 methanation activity is key towards better, more robust and thermally stable catalysts.

Acknowledgements

The authors thank Monique Riendeau for conducting the N_2 adsorption/desorption and Ranjan Roy and Andrew Golsztajn for the ICP-OES measurements. The authors acknowledge the financial support from the Natural Sciences and Engineering Research Council of Canada (NSERC, RGPIN/04685-2014).

References

[1] M. Götz, J. Lefebvre, F. Mörs, A. McDaniel Koch, F. Graf, S. Bajohr, R. Reimert, T. Kolb, Renew. Energy 85 (2016) 1371–1390.

[2] G.A. Mills, F.W. Steffgen, Catal. Rev. 8 (1974) 159–210.

[3] G.D. Weatherbee, C.H. Bartholomew, J. Catal. 68 (1981) 67–76.

[4] J.H. Chiang, J.R. Hopper, Ind. Eng. Chem. Prod. Res. Dev. 22 (1983) 225–228.

[5] J. Kopyscinski, T.J. Schildhauer, S.M.A. Biollaz, Fuel 89 (2010) 1763–1783.

[6] L. Xu, H. Zhao, H. Song, L. Chou, Int. J. Hydrogen Energy 37 (2012) 7497–7511.

[7] Q. Ma, J. Sun, X. Gao, J. Zhang, T. Zhao, Y. Yoneyama, N. Tsubaki, K. Tomishige, G. Xu, F. Su, N. Tsubaki, Catal. Sci. Technol. 6 (2016) 6542–6550.

[8] L. Xu, H. Song, L. Chou, Int. J. Hydrogen Energy 38 (2013) 7307–7325.

[9] K. Jabbour, N. El Hassan, A. Davidson, S. Casale, P. Massiani, Catal. Sci. Technol. 6 (2016) 4616–4631.

[10] Z.-X. Li, F.-B. Shi, L.-L. Li, T. Zhang, C.-H. Yan, Phys. Chem. Chem. Phys. 13 (2011) 2488–2491.

[11] C. Ding, W. Liu, J. Wang, P. Liu, K. Zhang, X. Gao, G. Ding, S. Liu, Y. Han, X. Ma, Fuel 162 (2015) 148–154.

[12] L. Xu, F. Wang, M. Chen, J. Zhang, K. Yuan, L. Wang, K. Wu, G. Xu, W. Chen, L.C. Chen, RSC Adv. 6 (2016) 28489–28499.

[13] S.M. Morris, P.F. Fulvio, M. Jaroniec, J. Am. Chem. Soc. 130 (2008) 15210–15216.

[14] W. Li, Q. Yue, Y. Deng, D. Zhao, Adv. Mater. 25 (2013) 5129–5152.

[15] D. Zhao, Y. Wan, W. Zhou, Ordered Mesoporous Materials, Wiley-VCH Verlag GmbH & Co. KGaA, Weinheim, Germany, 2013.

[16] N.A. Melosh, P. Lipic, F.S. Bates, F. Wudl, G.D. Stucky, G.H. Fredrickson, B.F. Chmelka, Macromolecules 32 (1999) 4332–4342.

[17] H. Lin, C. Kao, C. Mou, S. Liu, J. Phys. Chem. B 104 (2000) 7885–7894.

[18] N. Wang, K. Shen, L. Huang, X. Yu, W. Qian, W. Chu, ACS Catal. 3 (2013) 1638–1651.

[19] S. Fujita, M. Nakamura, T. Doi, N. Takezawa, Appl. Catal., A 104 (1993) 87–100.

[20] F. Koschany, D. Schlereth, O. Hinrichsen, Appl. Catal. B Environ. 181 (2016) 504–516.

[21] Z.A. Ibraeva, N. V Nekrasov, B.S. Gudkov, V.I. Yakerson, Z.T. Beisembaeva, E.Z. Golosman, Theor. Exp. Chem. 26 (1991) 584–588.

[22] Q. Pan, J. Peng, T. Sun, S. Wang, S. Wang, Catal. Commun. 45 (2014) 74–78.

[23] L. Xu, F. Wang, M. Chen, H. Yang, D. Nie, L. Qi, X. Lian, RSC Adv. 7 (2017) 18199–18210.

List of Tables

Table 1 Sample overview: Synthesis parameter (target Ni loading, calcination temperature T_{cal}, acid used) and N_2 adsorption/desorption results (total and mesoporous surface area, average pore size, pore volume).

Table 2 Target and actual nickel loadings for ordered mesoporous catalysts determined by ICP-OES.

Table 3 H_2-uptake [µmol g^{-1}], specific surface area [m^2 g^{-1}], average nickel crystallite size [nm] and metal dispersion [%].

Table 4 BET surface area analysis for fresh and spent catalysts.

List of Figures

Fig. 1 Top row: N_2 adsorption/desorption isotherms and bottom row: pore size distribution for catalysts synthesized with (A, B) various acids, (C-F) different calcination temperatures and (G, H) different nickel loadings.

Fig. 2 TEM of fresh OMA-15Ni-500; (A) scale 200 nm, (B) scale 50 nm and (C) scale 5 nm including crystallite size distribution.

Fig. 3 H_2-TPR results for OMA catalysts synthesized with different (A) calcination temperatures and (B) nickel loadings.

Fig. 4 XRD patterns of the nickel containing OMA catalysts synthesized with (A) different methods (i.e., with HNO_3, HCl, and wet impregnation; OMA-15Ni-500, OMA-15Ni-500 HCl, and 15Ni/OMA-500, respectively), (B) different calcination temperatures, and (C) different nickel loadings. Reference patters of $NiAl_2O_4$, NiO and γ-Alumina are PDF #010-0339, PDF #044-1159, and PDF #050-074, respectively.

Fig. 5 XRD patterns of OMA-30Ni-500 after drying, calcination and reduction. Reference patters of NiO and Ni are PDF #044-1159 and PDF #04-010-6148, respectively.

Fig. 6 (A) Conversion of CO_2 and (B) selectivity of CH_4 as a function of reaction temperature for catalysts synthesized with HCl, HNO_3, and wet impregnation; OMA-15Ni-500 HCl, OMA-15Ni-500 and 15Ni/OMA-500, respectively (all catalyst calcined at 500°C). Symbols denote experimental data; solid orange line denotes chemical equilibrium; dotted lines are for guidance only.

Fig. 7 Mass spectrum of the reaction products for experiments conducted at 350°C and 450°C over OMA-15Ni-500 catalyst.

Fig. 8 (A) Conversion of CO_2 and (B) selectivity of CH_4 as a function of reaction temperature for catalysts synthesized at different calcination temperatures (i.e., from 400 to 900°C). Symbols denote experimental data; solid orange line denotes chemical equilibrium; dotted lines are for guidance only.

Fig. 9 (A) Conversion of CO_2 and (B) selectivity of CH_4 as a function of reaction temperature for catalysts synthesized at different nickel loading (i.e., from 5 to 30 wt%). Symbols denote experimental data; solid orange line denotes chemical equilibrium; dotted lines are for guidance only.

Fig. 10 (A) Conversion of CO_2 and (B) selectivity of CH_4 as a function of GHSV and reaction temperature for the OMA-15Ni-700 catalyst.

Fig. 11 Comparison of XRD patterns of fresh and used catalyst. Reference patters of NiO and Ni are PDF #044-1159 and PDF #04-010-6148, respectively.

Fig. 12 (A) Conversion of CO_2 and selectivity of CH_4 as a function of time for the OMA-15Ni-700 catalyst with H_2/CO_2 = 5/1, GHSV = 91 $L_N\ g_{cat}^{-1}\ h^{-1}$ and T = 400°C. (B) TGA-TPO results for the OMA-15Ni-700 catalyst before and after the long-term test.

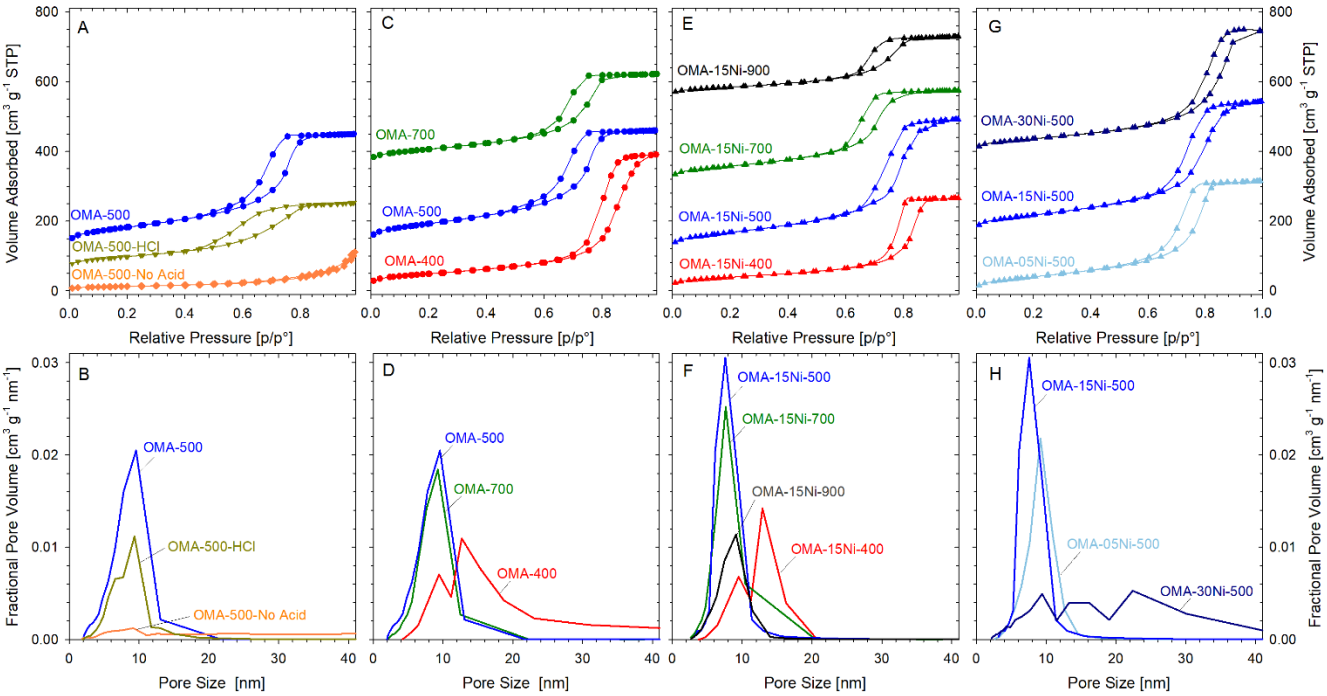
A
C
E
G
B
D
F
H
OMA-500
OMA-500-HCl
OMA-500-No Acid
OMA-700
OMA-400
OMA-15Ni-900
OMA-15Ni-700
OMA-15Ni-500
OMA-15Ni-400
OMA-30Ni-500
OMA-05Ni-500
Volume Adsorbed [cm^3 g^{-1} STP]
Relative Pressure [p/p°]
Fractional Pore Volume [cm^3 g^{-1} nm^{-1}]
Pore Size [nm]

Fig. 1

514 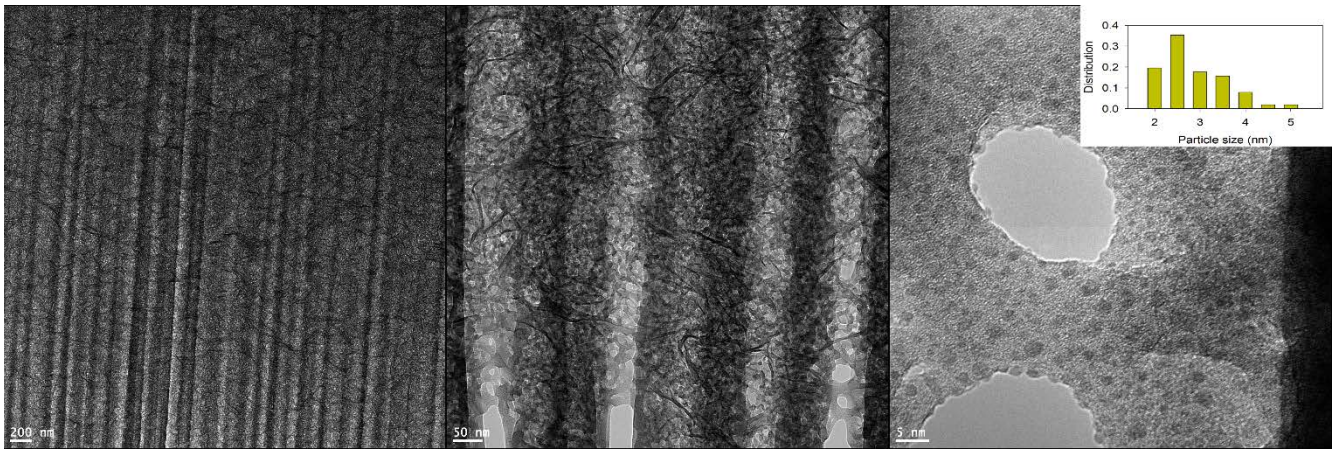

515 Fig. 2

516

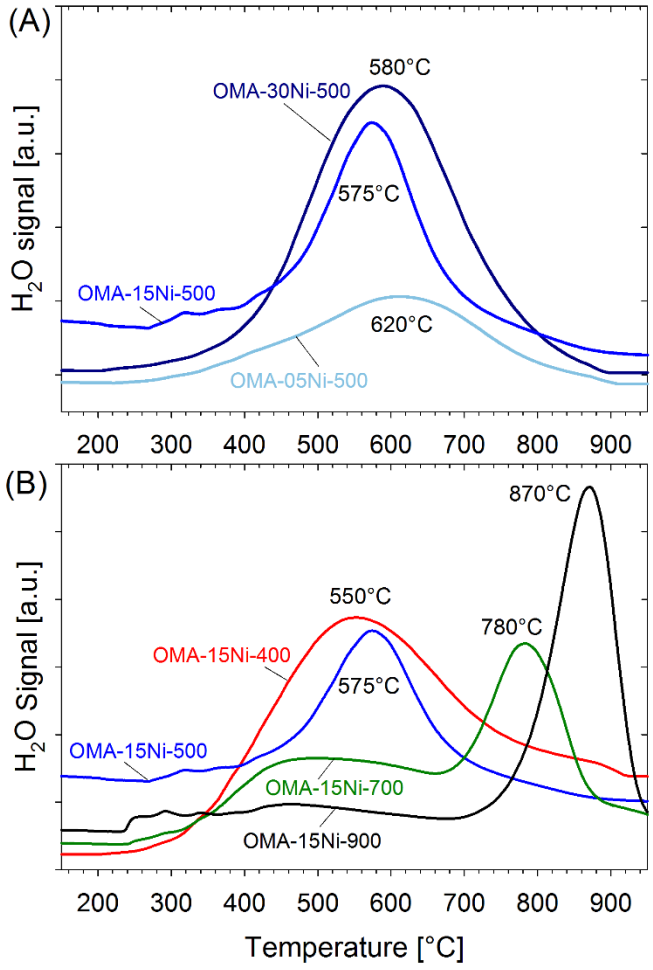

517

518 Fig. 3

519

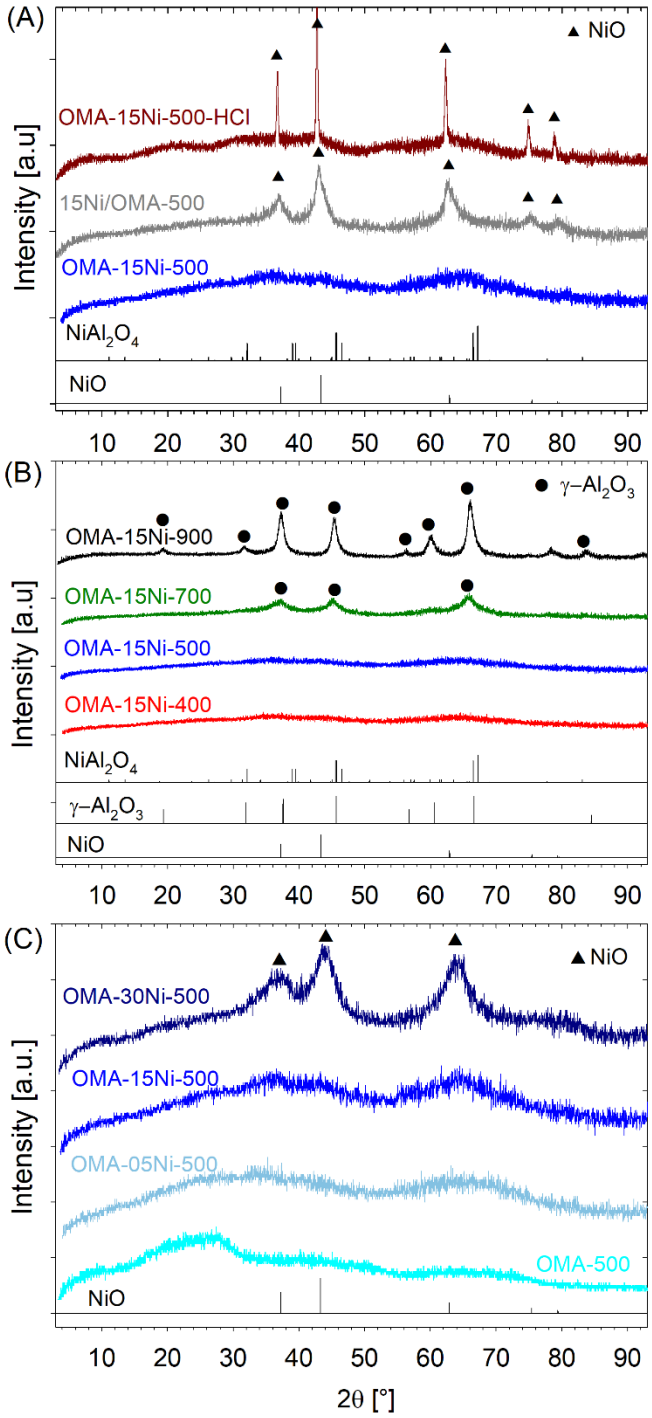
(A)
▲ NiO
OMA-15Ni-500-HCl
15Ni/OMA-500
OMA-15Ni-500
NiAl2O4
NiO
Intensity [a.u]
10 20 30 40 50 60 70 80 90
(B)
● γ–Al2O3
OMA-15Ni-900
OMA-15Ni-700
OMA-15Ni-500
OMA-15Ni-400
NiAl2O4
γ–Al2O3
NiO
Intensity [a.u]
10 20 30 40 50 60 70 80 90
(C)
▲ NiO
OMA-30Ni-500
OMA-15Ni-500
OMA-05Ni-500
OMA-500
NiO
Intensity [a.u.]
10 20 30 40 50 60 70 80 90
2θ [°]

Fig. 4

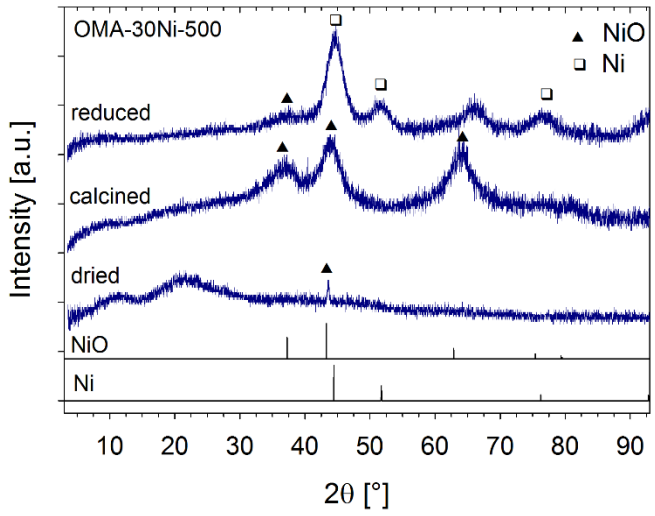

523

524 Fig. 5

525

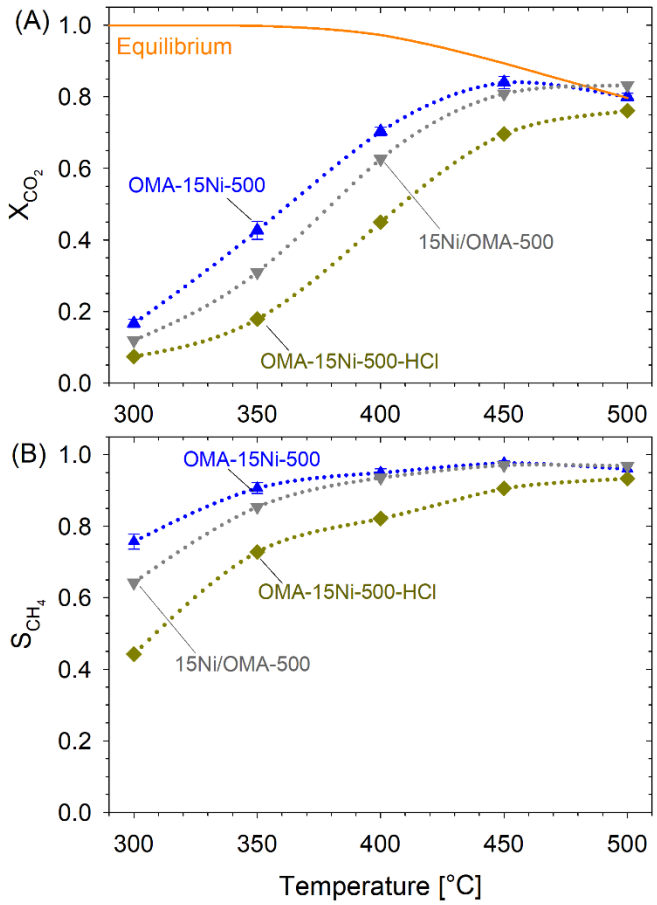

526

527 Fig. 6

528

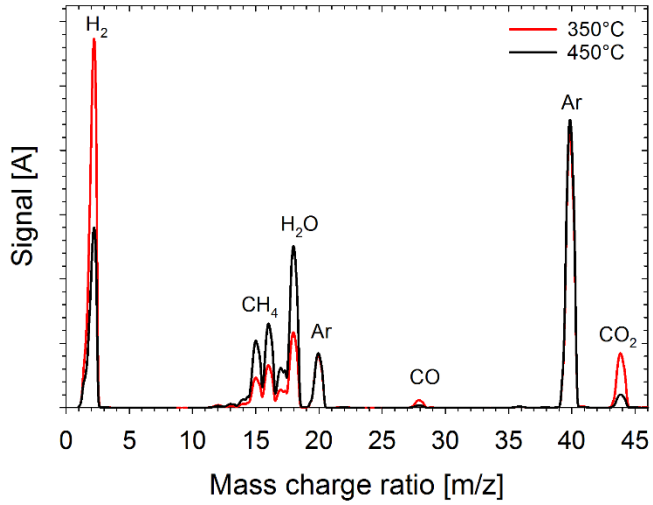

529

530 Fig. 7

531

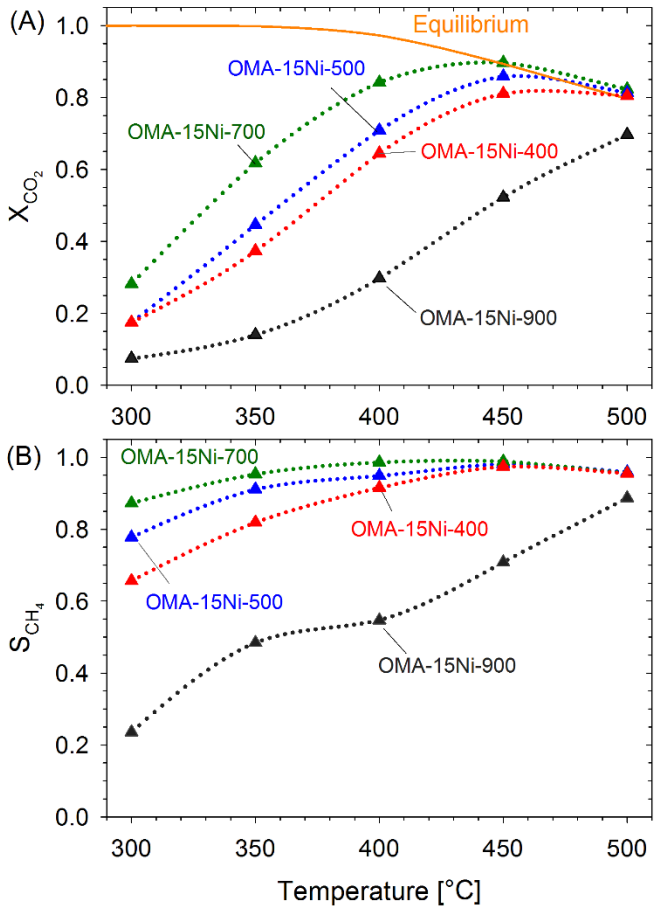

532

533 Fig. 8

534

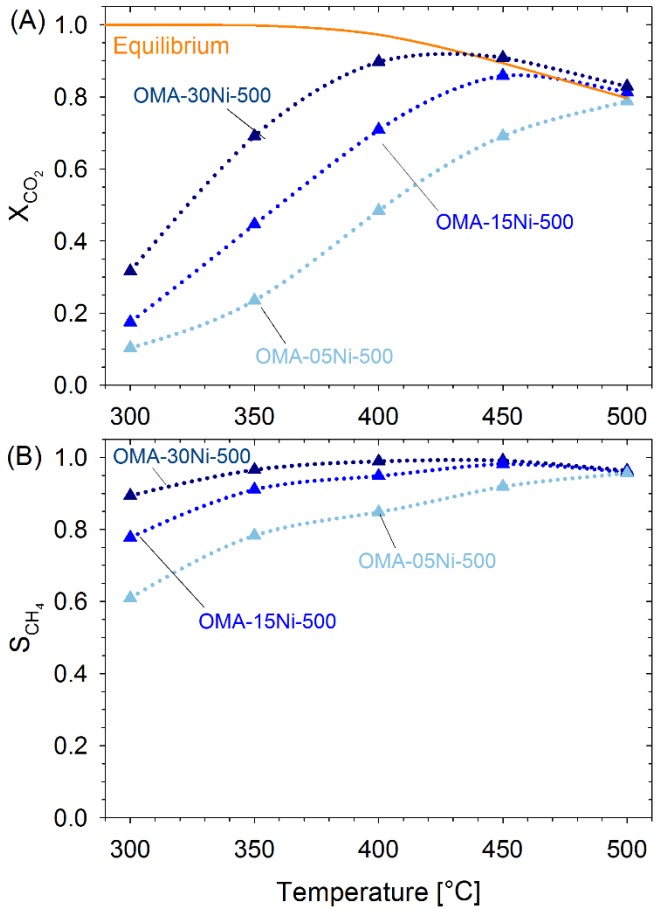

535

536 Fig. 9

537

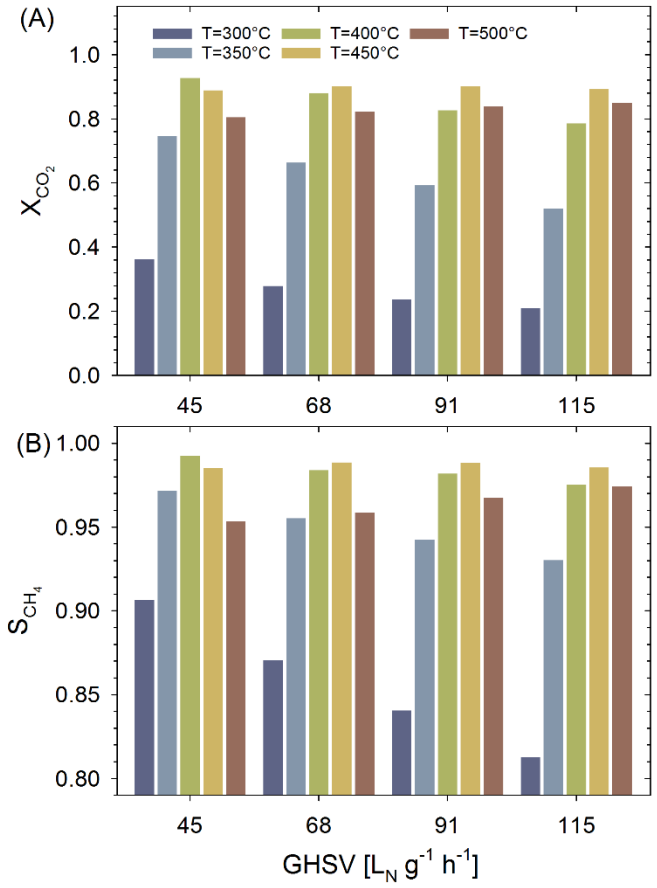

538

539 Fig. 10

540

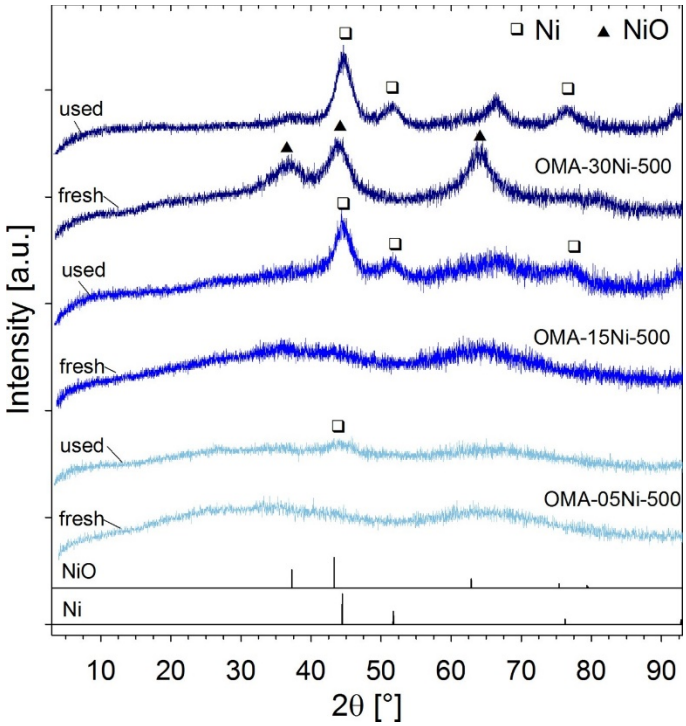
Ni
NiO
used
fresh
OMA-30Ni-500
used
fresh
OMA-15Ni-500
used
fresh
OMA-05Ni-500
NiO
Ni
Intensity [a.u.]
10
20
30
40
50
60
70
80
90
2θ [°]

Fig. 11

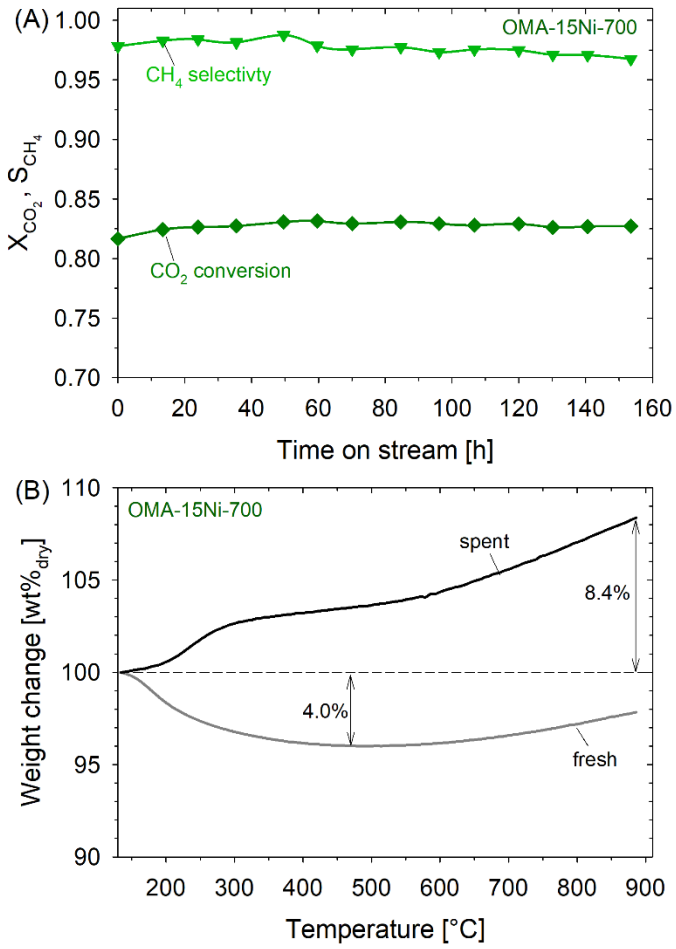

543

544 Fig. 12